Supplementary Information for

Deglacial increase of temperature variability in the tropical ocean

Lars Wörmer, Jenny Wendt, Brenna Boehman, Gerald H. Haug, Kai-Uwe Hinrichs.

Correspondence to: lwoermer@marum.de

Supplementary Information

S1. Decadal to centennial scale SST changes during the YD-Holocene transition and in the early Holocene

Regarding centennial scale trends, reconstructed SST (average SST = 24.3 °C) remains relatively stable during the YD-Holocene transition. At ~11.4 kyr b2k a warming trend is observed, SST increases from an average 23.9 °C before 11.39 kyr b2k to an average 25.5 °C after 11.37 kyr b2k. Trends identified by MSI are consistent with conventional $U^{K'}_{37}$ analyses performed in the present study and those previously reported by Herbert and Schuffert[1] on ODP core 165-1002C (Extended Data Fig. 1). These authors observed a slight warming several hundred years after the transition into the Holocene, between ~11.53 and 11.32 kyr b2k.

Three prominent SST maxima are observed between ~11.50 to 11.45 kyr b2k. Average SST in these 50 years is 1.3 °C higher than in the 50 years before and after. These maxima are synchronous with the 11.4 ka cold event or Preboreal Oscillation (PBO) characterized by a negative excursion in $\delta^{18}O$ and reduced snow accumulation rates in Greenland ice cores[2] (Extended Data Fig. 2). The PBO coincides with the oldest of the Bond events, i.e., pulses of ice rafting in the Northern Atlantic indicative of climatic deterioration[3].

A warm tropical response to the PBO would be supported by the lower resolution foraminiferal SST record of Lea et al. [4], which shows two data points of increased SST shortly after the end of the YD-Holocene transition. To enable direct comparison, ages in Lea et al. [4] were corrected for the age difference between the sediment color based YD termination midpoint in their record and in data from Deplazes et al. [5]. After this correction, these maxima correspond to 11.43 and 11.50 kyr b2k (Extended Data Fig. 2). Further, the SST maxima coincide with a short-lived change to lighter-colored sediments. Hughen et al. [6] described a correlation between

brief North Atlantic cold events, like the PBO, and changes in tropical primary productivity mediated by stronger upwelling that result in lighter sediments in the Cariaco Basin. Far-reaching effects of PBO have previously been described in West Asia, with increased dust plumes being related to a southward shift of the westerlies[7].

The identification of the mechanisms behind a potential Tropical North Atlantic (TNA) response to PBO is beyond the scope of this study. We want to point out, however, that high resolution records are crucial to identify such events, and to differentiate between underlying changes coinciding in time and, as in the present case, sharp signals that act on the same multi-decadal timescales and can potentially be triggered by the same processes[8].

S2. The effect of changing sedimentation rate on reconstructed ENSO variability during the YD-Holocene transition

Pooling proxy data into 1-yr horizons establishes a constant sampling rate and thereby prevents potential effects of changing sedimentation rates. The onset of the Holocene in the Cariaco Basin sediments is characterized by a sharp decrease in sedimentation rates from 1.4 to 0.5 mm yr^{-1} [5,6]. Consequently, in the yearly pooled data we observe a reduction in the number of values summed up for each horizon (Extended Data Fig. 9), as fewer laser spots fit into the thinner Holocene annual layers. At the same time, the mean intensity in each of these spots slightly increases, consistent with a relative increase of the contribution of haptophytes to primary production[9].

We have previously shown that precision of MSI-based molecular proxy analysis is dependent on both the number of spots pooled per data-point and the signal intensity in these spots[10]. All horizons used in the downcore record are above the established threshold of 10 spots, and proxy variability was shown to stabilize above this threshold[10,11]. However, as a decrease in

the number of values per horizon might still result in lower analytical precision and contribute to higher signal variability, we corrected variability in the 2-8 yr window with the estimated analytical variability (see method section, equation 3). With this correction, the magnitude of the described variability decreases across the record, but the trend towards higher interannual variability in the Holocene persists (Fig. 2C).

S3. Varve formation and alkenone deposition in the sediments of the Cariaco Basin during the YD-Holocene transition

Comparison of elemental maps and sediment color (Extended Data Fig. 5) reveals a consistent pattern of lamination across the YD-Holocene transition that results from the seasonal interplay of precipitation, upwelling and dominant phytoplankton community composition. Darker laminae represent the rainy, non-upwelling (summer/fall) season and are enriched in Fe and Ti from terrigenous material and Ca sourced from biogenic $CaCO_3$ produced by foraminifera or coccolithophores. Lighter laminae are characterized by high abundance of Si and correspond to the increased production of biogenic opal by diatoms during the upwelling (winter/spring) season[12]. This is in agreement with observations by Hughen et al.[13], who described the laminae couplets in the Cariaco Basin as representing annual cycles, whereby light laminae are an indicator of high productivity associated with the winter-spring upwelling season and dark laminae an indicator of summer/fall runoff and accumulation of terrigenous material. Deplazes et al.[14] described a divergent origin of lamination for a deeper section of the YD, with light laminae being rich in calcareous and terrigenous elements characteristic for the summer season, while dark layers were enriched in Si and Br, indicative of diatoms and organic-walled primary producers characteristic for the more productive winter season. Such an alteration of the characteristic pattern of lamination is not observed in the late YD investigated here.

This blueprint of seasonality was used to assess seasonal behavior of alkenones. Alkenones were deposited throughout the year, as evidenced by the fact that the number of spots containing detectable amounts of both alkenone species are not restricted to the upwelling or non-upwelling season, but distributed across a relatively wide range of GS values to both sides of the median (Extended Data Fig. 6). Average alkenone signal intensity is higher in the non-upwelling season, pointing to a preference of alkenone producers for this season and/or to a stronger dilution of the signal in the upwelling season. Regarding the $U^{K'}_{37}$ SST proxy distribution in light versus dark layers, our observations are in agreement with the ability to capture the seasonal SST cycle with alkenones in sinking particles in the modern Cariaco Basin[15].

S4. Effect of changing seasonality on YD and early Holocene SST records from the western TNA

Changing seasonality can contribute to explain contrasting lower resolution SST records in the western TNA during the YD and the early Holocene. The strong warming during the YD-Holocene transition recorded in the foraminiferal Mg/Ca record of the Cariaco Basin (Lea et al.[4], Extended Data Fig 1) might be reflecting the more robust thermohaline stratification and increasingly warmer non-upwelling seasons, given the preference of *Globigerinoides ruber* for this season.

G. ruber (white), as employed by Lea et al.[4], is considered to be a dominant species in the tropics, with a relatively uniform annual distribution. However, in the modern Cariaco Basin, upwelling leads to a distinct foraminiferal community composition and seasonal turnover[16], consistent with the notion of warm-water foraminifera narrowing their occurrence to the warmest season[17]. Relative abundance of *G. ruber* increases in the non-upwelling (warm) season but rarely exceeds 15%, while the upwelling season is clearly dominated by *G. bulloides*[18,19]. *G. ruber*

fluxes are consistently lowest when upwelling is most vigorous, as expressed in annual minima in SST (Extended Data Fig. 10). As upwelling during the YD and early Holocene was more intense than in the present[16], the preference of *G. ruber* for the summer (non-upwelling) season might have been even more pronounced.

The development of a stronger seasonality in the early Holocene would thus have led to a narrower temporal occurrence of *G. ruber* in the non-upwelling season, during which it would additionally be exposed to higher SST. The average SST difference between seasons obtained in our analysis can be converted into annual SST amplitude by assuming a sinusoidal curve. By doing so we observe an increase in the seasonal amplitude of 1.5 to 1.9°C (depending on the ramp fitted), which is similar to the warming described in Lea et al.[4].

This interpretation is in agreement with Bova et al.[20] who observed that most Holocene climate reconstructions are biased towards the boreal summer/fall and reflect the evolution of seasonal rather than annual temperatures. As discussed above, this is probably not true for the $U^{K'}_{37}$ index in the Cariaco Basin, as alkenones are deposited throughout the year. The suggested weakening of summer stratification during the YD (as compared to the Holocene) might however explain why the lower resolution $U^{K'}_{37}$ records from the semi-enclosed Cariaco Basin show no or weaker warming[1] than other, open-ocean, tropical YD records[21], where the interplay of upwelling, freshwater input and stratification are less relevant to the SST signal.

Extended Data Figures

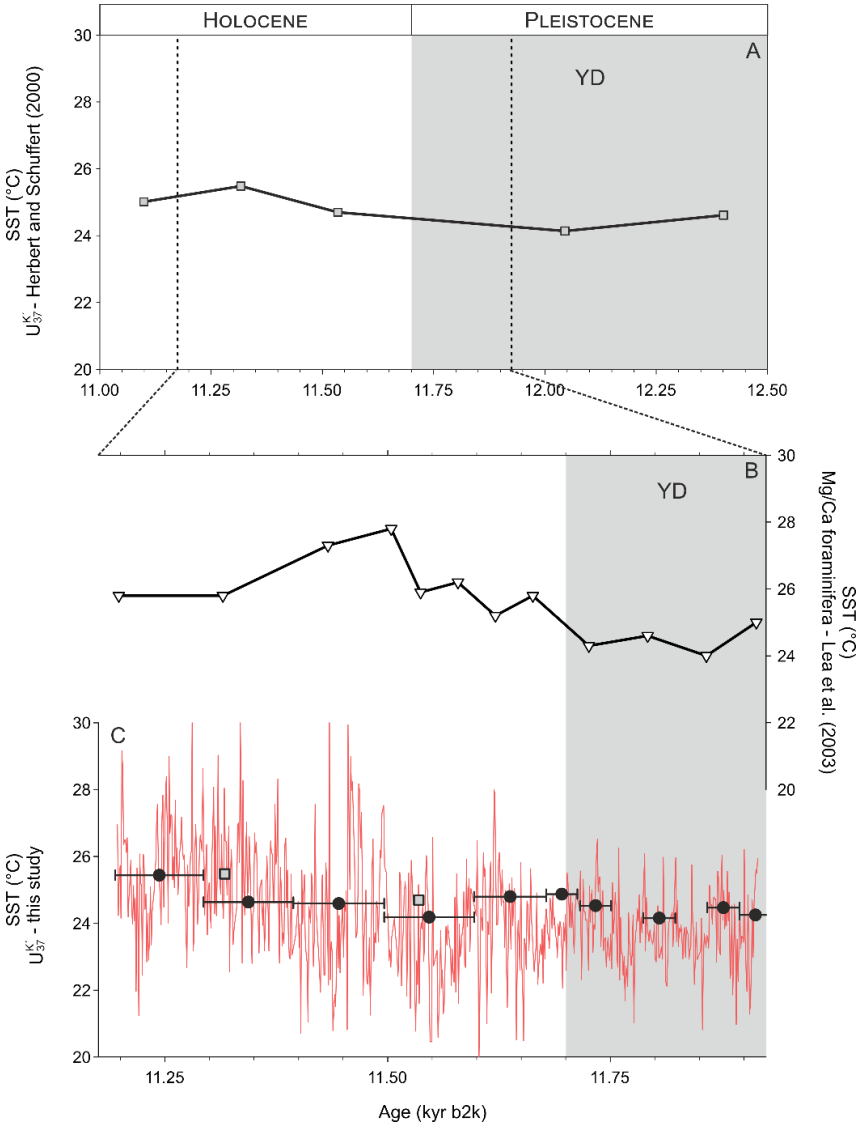

Extended Data Fig. 1.

Comparison of MSI-based and conventional SST records in the Cariaco Basin. (**A**) Reconstructed SST from Herbert and Schuffert[1] based on the $U^{K'}_{37}$ proxy. The updated age model from Haug et al.[22] was applied and expressed in kyr b2k to make the record comparable to our data. (**B, C**) Zoom-in to the YD-Holocene transition investigated in the present study. (B) Foraminifera-based SST reconstruction in the Cariaco Basin[4]. Ages were adjusted by normalizing to the respective

midpoints of the YD-Holocene transition expressed as changes in sediment color in Deplazes et al.[5] and Lea et al.[4]. (C) MSI-based reconstruction (red line) shown together with data obtained by extracting sediment slices after having been used for MSI (black circles) and the two data points from the Herbert and Schuffert[1] study that fall into the investigated interval (gray squares). Horizontal bars indicate the age interval corresponding to the data pooled into each extraction.

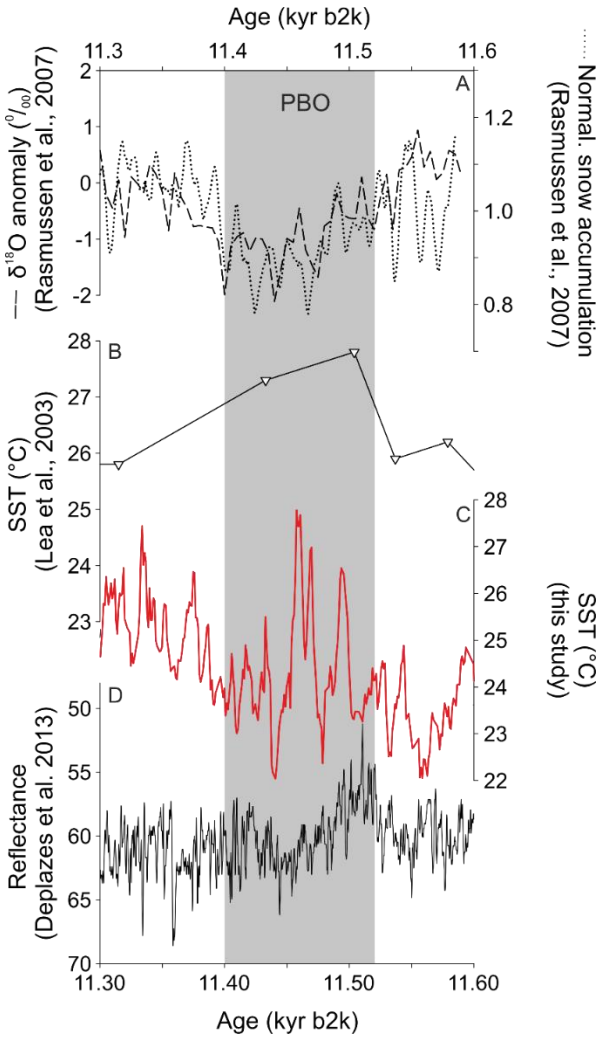

Extended Data Fig. 2.

Evidence for a tropical response during the PBO. (**A**)The PBO is expressed as a negative excursion in $\delta^{18}O$ and reduced snow accumulation rates in Greenland ice cores[2]. (**C**) Abrupt SST maxima in our record are consistent with (**B**) lower resolution SST reconstruction[4] and are accompanied by (**D**) an increase in reflectance indicative of changes in upwelling intensity[5]. Duration of the PBO (11.52 – 11.40 kyr b2k) as defined by Rasmussen et al.[23].

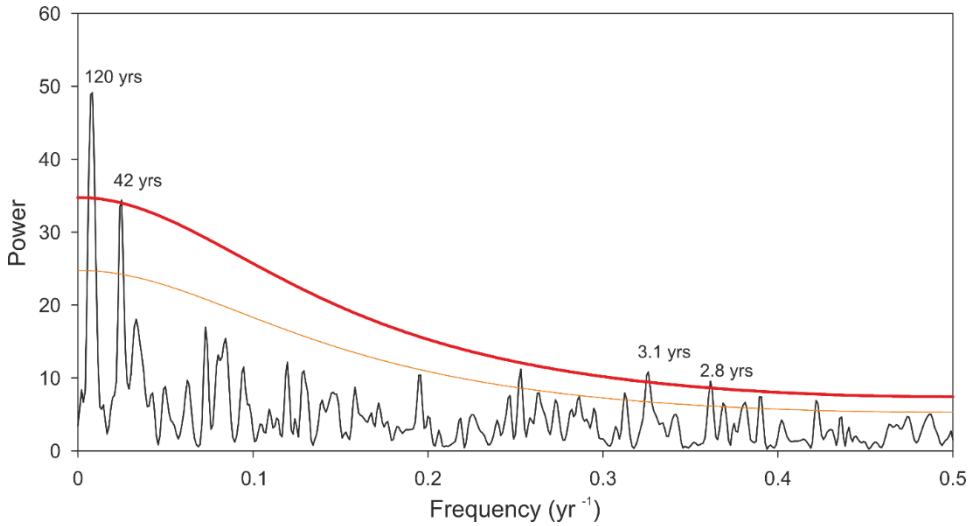

Extended Data Fig. 3.

Spectral analysis of the annually resolved SST record. Thick red and thin orange lines are 99% and 95% significance levels against red noise.

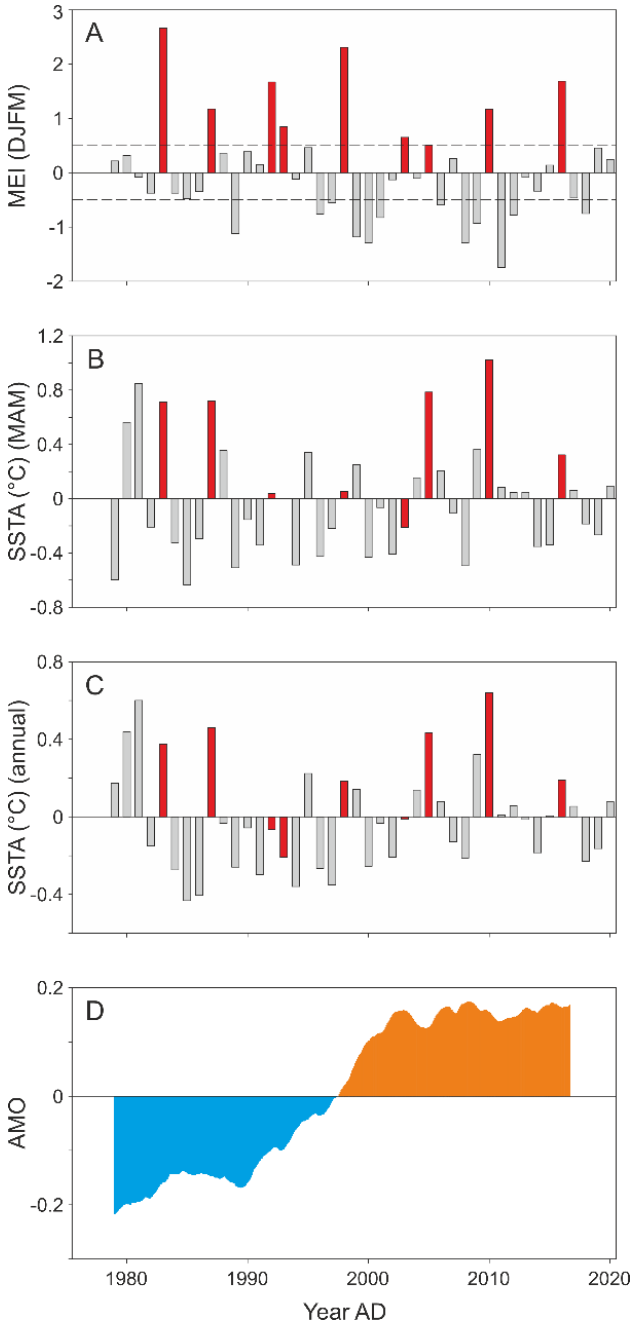

Extended Data Fig. 4

Teleconnection of ENSO to the Cariaco Basin. (**A**) Positive ENSO events identified by the MEI.v2 index (https://psl.noaa.gov/enso/mei/) are marked in red and lead to positive spring (**B**) and annual (**C**) sea surface temperature anomalies (SSTA) in the Cariaco Basin. SSTA are calculated from HadISST[24]. Four from the five (six) strongest positive spring (annual) SST

anomalies were related to positive ENSO events. From the nine positive ENSO events detected, eight (six) resulted in positive spring (annual) SST anomalies. The effect of positive ENSO was muted between the years 1992 and 2003, coinciding with (**D**) a shift from negative to positive AMO[25], which is consistent with TNA-wide neutral response to positive ENSO events in 1992 and 2003[26] and with a dependency of the ENSO teleconnection to AMO state[27].

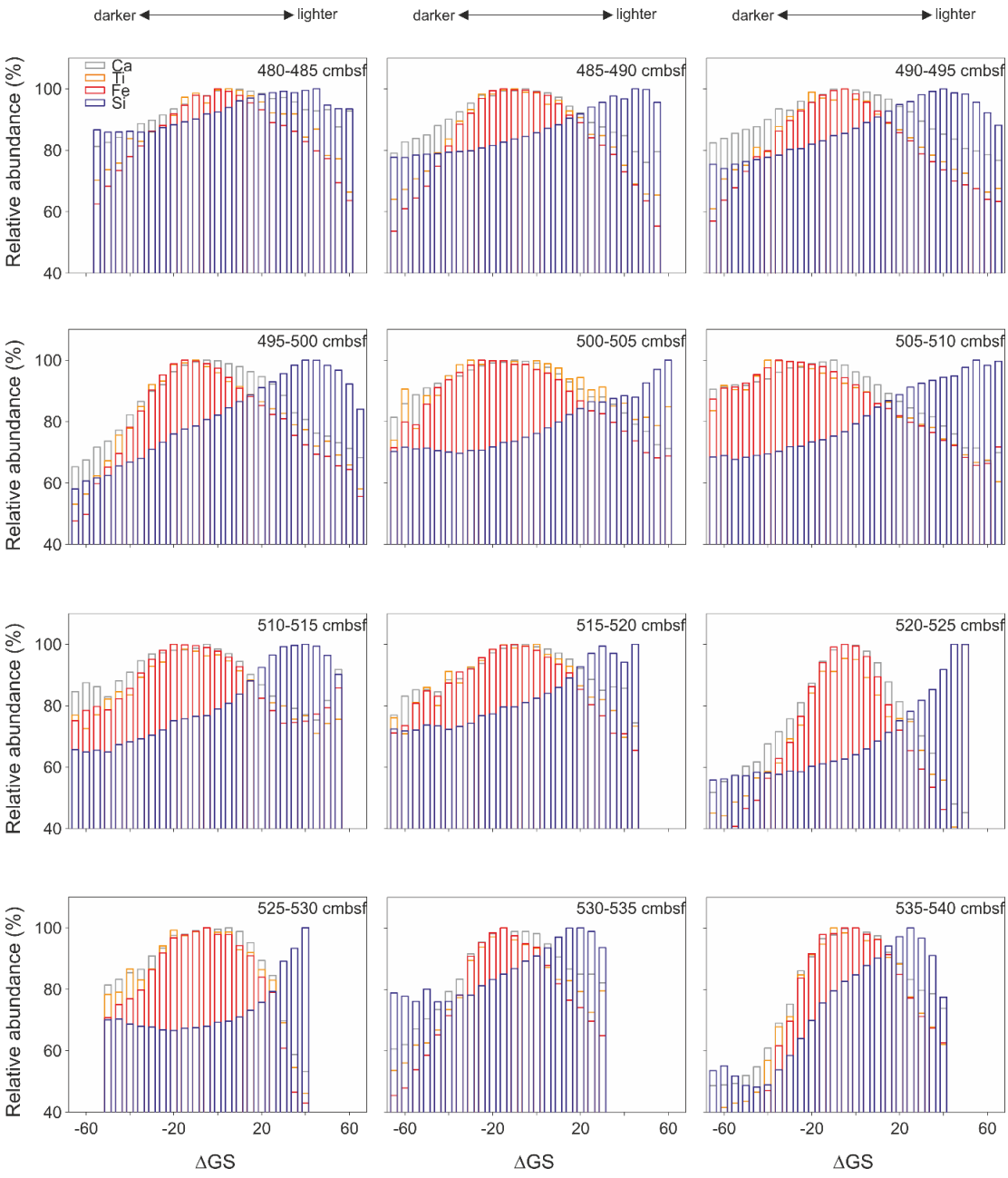

Extended Data Fig. 5.

Elemental composition binned according to sediment color for each 5-cm piece analyzed. Sediment color is presented as delta grayscale (ΔGS, i.e. the difference to the mean GS value of each sample). Counts for each element were averaged for every bin and normalized to the highest value. Only bins with at least 100 data points were considered. The YD/Holocene transition, as defined by the change in sediment color[5], is situated between 501 and 509 cmbsf.

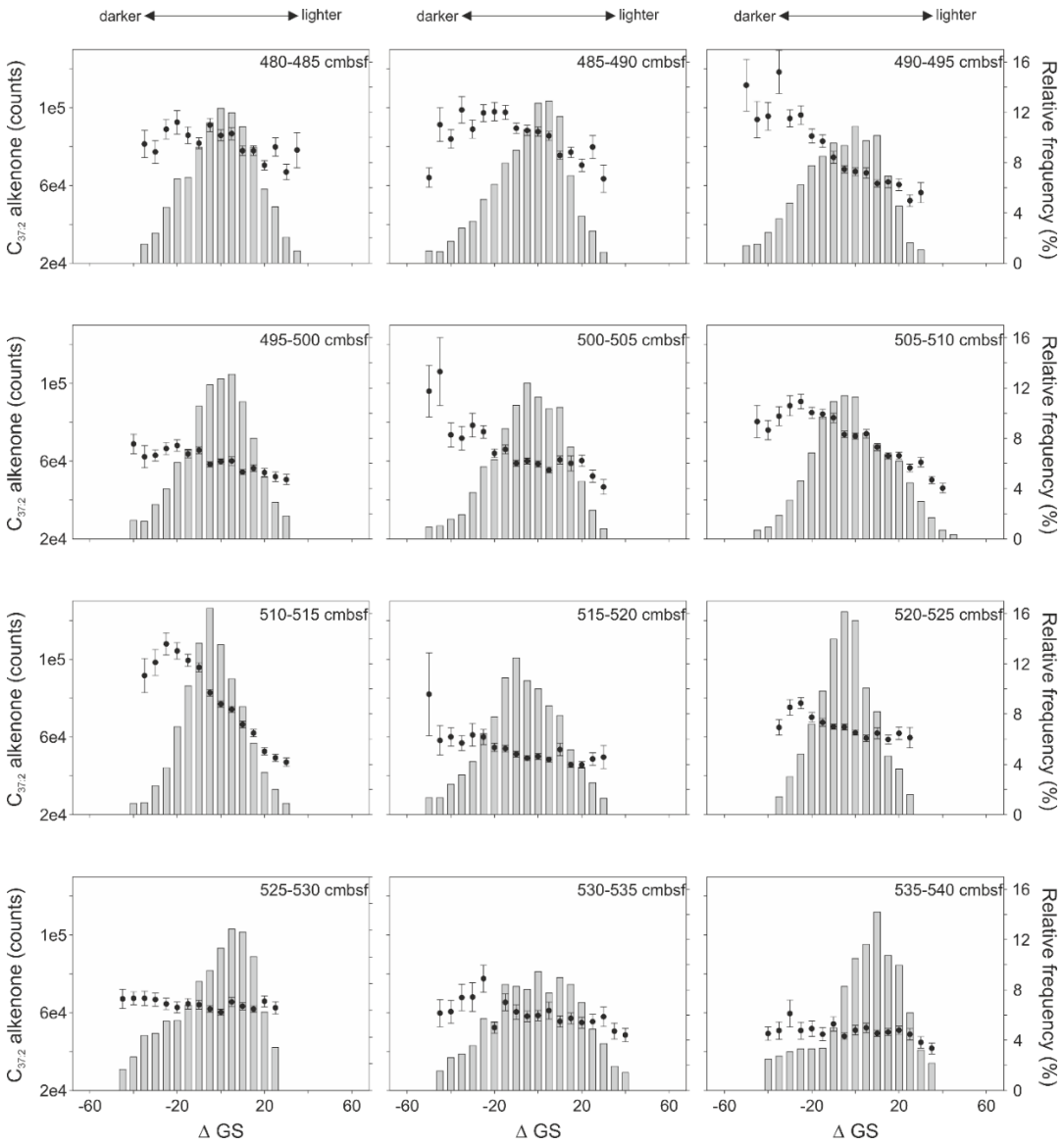

Extended Data Fig. 6.

$C_{37:2}$ long chain alkenone intensity binned according to sediment color for each 5-cm piece analyzed (black dots) and relative contribution of each bin to the total number of spots in which both alkenones used in the $U^{K'}_{37}$ proxy were detected (gray bars). Sediment color is presented as delta grayscale (ΔGS; i.e., the difference to the mean GS value of each sample). Mean and standard error of alkenone intensity are shown. Only bins with at least 25 data points are shown. The YD/Holocene transition, as defined by the change in sediment color[5], is situated between 501 and 509 cmbsf.

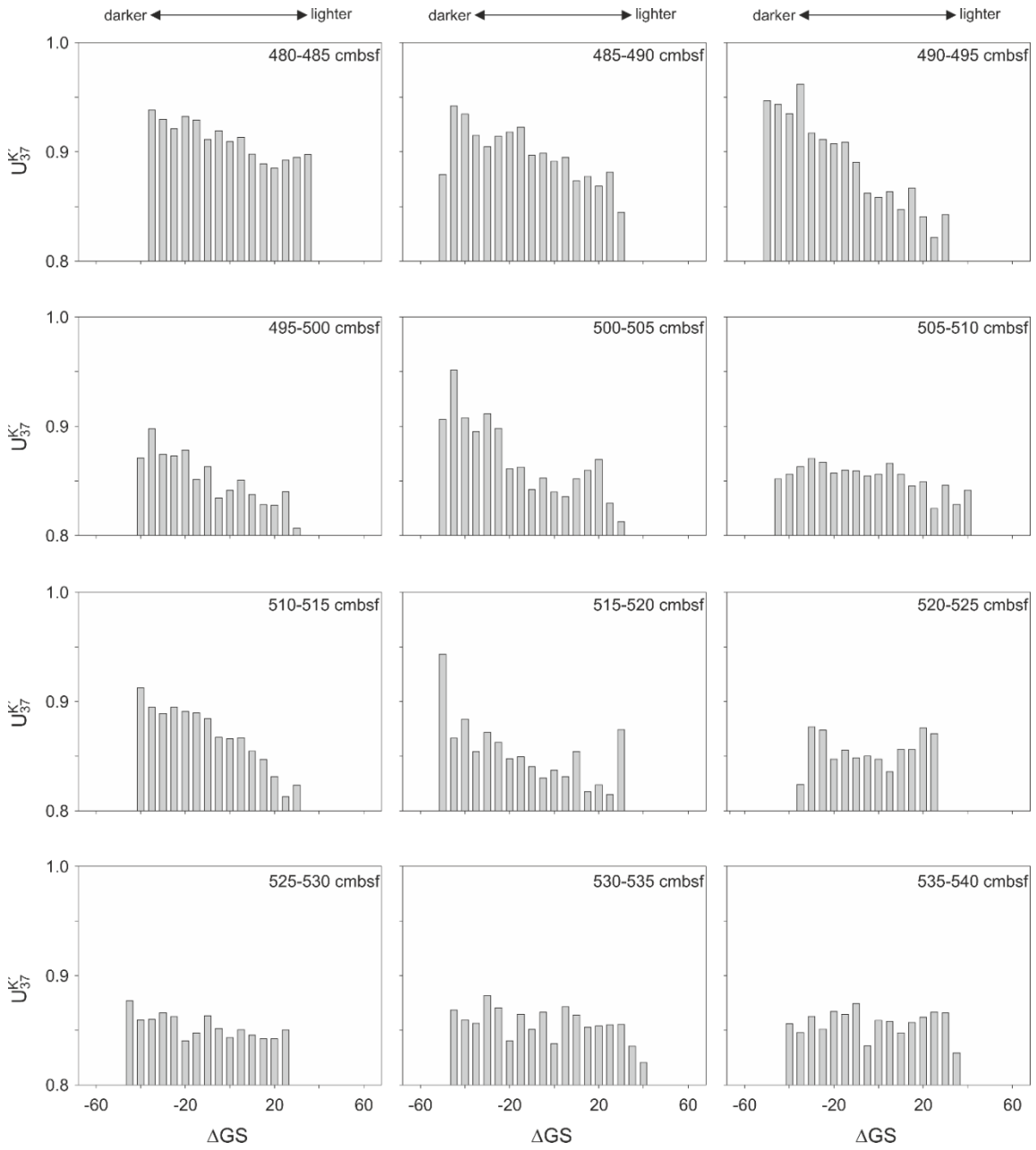

Extended Data Fig. 7.

$U_{37}^{K'}$ values binned according to sediment color for each 5-cm piece analyzed. Sediment color is presented as delta grayscale (ΔGS; i.e. the difference to the mean GS value of each sample). $U_{37}^{K'}$ was calculated based on the sum of intensities in each bin, and values obtained by MSI were converted to GC equivalents. Only bins with at least 25 data points are shown. The YD/Holocene transition, as defined by the change in sediment color[5], is situated between 501 and 509 cmbsf.

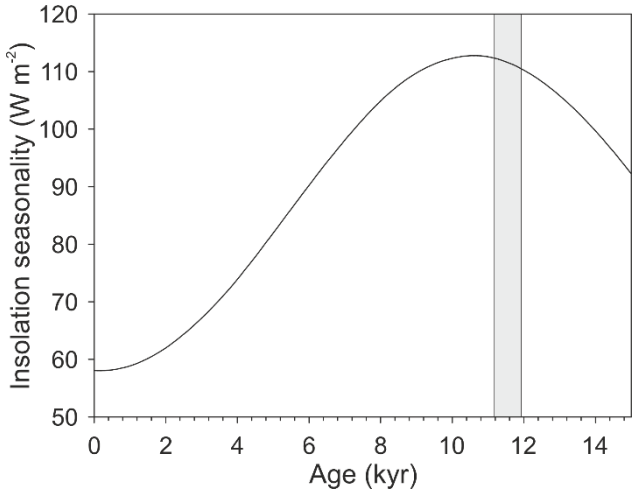

188

189 **Extended Data Fig. 8.**

190 Seasonality of insolation at 10°N calculated as the difference between summer (JJA) and winter

191 insolation (DJF) provided by Laskar et al.[28]. Shaded area indicates the investigated interval.

192

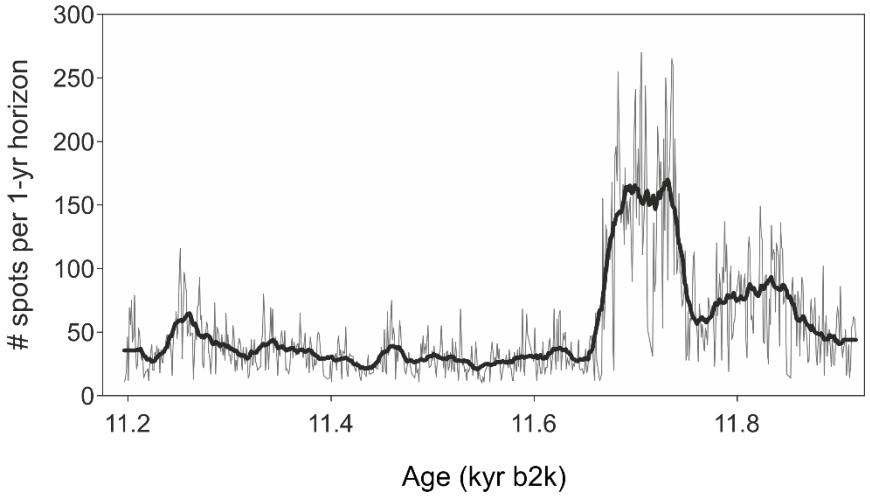

Extended Data Fig. 9.

Number of spots pooled in each 1-yr horizon to construct the $U_{37}^{K'}$ record. Thin gray line shows annual values, thick black line the 25-yr running mean.

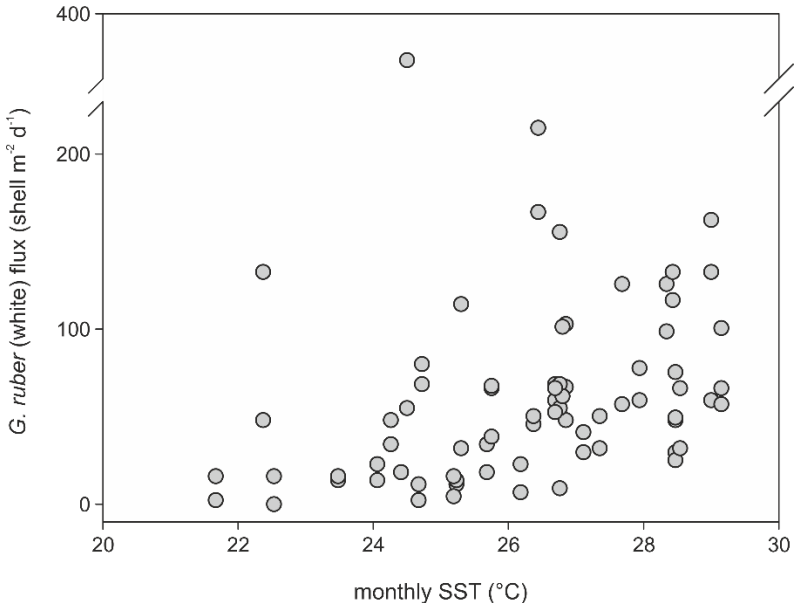

Extended Data Fig. 10.

Flux of *G. ruber* (white) in sediment traps from the Cariaco Basin plotted against monthly sea surface temperature (SST). All data from Tedesco and Thunell [19].

References

1 Herbert, T. D. & Schuffert, J. D. in *Proceedings of the Ocean Drilling Program, Scientific Results.* 239-247.

2 Rasmussen, S. O., Vinther, B. M., Clausen, H. B. & Andersen, K. K. Early Holocene climate oscillations recorded in three Greenland ice cores. *Quaternary Science Reviews* **26**, 1907-1914 (2007).

3 Bond, G. *et al.* A pervasive millennial-scale cycle in North Atlantic Holocene and glacial climates. *Science* **278**, 1257-1266 (1997).

4 Lea, D. W., Pak, D. K., Peterson, L. C. & Hughen, K. A. Synchroneity of tropical and high-latitude Atlantic temperatures over the last glacial termination. *Science* **301**, 1361-1364, doi:DOI 10.1126/science.1088470 (2003).

5 Deplazes, G. *et al.* Links between tropical rainfall and North Atlantic climate during the last glacial period. *Nature Geoscience* **6**, 213-217 (2013).

6 Hughen, K. A., Overpeck, J. T., Peterson, L. C. & Trumbore, S. Rapid climate changes in the tropical Atlantic region during the last deglaciation. *Nature* **380**, 51-54 (1996).

7 Safaierad, R. *et al.* Elevated dust depositions in West Asia linked to ocean–atmosphere shifts during North Atlantic cold events. *Proceedings of the National Academy of Sciences* **117**, 18272-18277 (2020).

8 Rohling, E. J. & Pälike, H. Centennial-scale climate cooling with a sudden cold event around 8,200 years ago. *Nature* **434**, 975-979 (2005).

9 Werne, J. P., Hollander, D. J., Lyons, T. W. & Peterson, L. C. Climate-induced variations in productivity and planktonic ecosystem structure from the Younger Dryas to Holocene in the Cariaco Basin, Venezuela. *Paleoceanography* **15**, 19-29, doi:Doi 10.1029/1998pa000354 (2000).

10 Wörmer, L. *et al.* Towards multiproxy, ultra-high resolution molecular stratigraphy: Enabling laser-induced mass spectrometry imaging of diverse molecular biomarkers in sediments. *Org. Geochem.* **127**, 136-145, doi:10.1016/j.orggeochem.2018.11.009 (2019).

11 Alfken, S. *et al.* Mechanistic insights into molecular proxies through comparison of subannually resolved sedimentary records with instrumental water column data in the Santa Barbara Basin, Southern California. *Paleoceanography and Paleoclimatology* **35**, e2020PA004076 (2020).

12 Romero, O. E., Thunell, R. C., Astor, Y. & Varela, R. Seasonal and interannual dynamics in diatom production in the Cariaco Basin, Venezuela. *Deep Sea Research Part I: Oceanographic Research Papers* **56**, 571-581 (2009).

13 Hughen, K. A., Overpeck, J. T., Peterson, L. C. & Anderson, R. F. The nature of varved sedimentation in the Cariaco Basin, Venezuela, and its palaeoclimatic significance. *Geological Society, London, Special Publications* **116**, 171-183 (1996).

14 Deplazes, G. *et al.* Fingerprint of tropical climate variability and sea level in sediments of the Cariaco Basin during the last glacial period. *Sedimentology* **66**, 1967-1988, doi:10.1111/sed.12567 (2019).

15 Turich, C. *et al.* Comparison of TEX86 and U37K′ temperature proxies in sinking particles in the Cariaco Basin. *Deep Sea Research Part I: Oceanographic Research Papers* **78**, 115-133 (2013).

16 Peterson, L. C., Overpeck, J., Kipp, N. & Imbrie, J. A high-resolution late Quaternary upwelling record from the anoxic Cariaco Basin, Venezuela. *Paleoceanography* **6**, 99-119 (1991).
17 Jonkers, L. & Kučera, M. Global analysis of seasonality in the shell flux of extant planktonic Foraminifera. *Biogeosciences* **12**, 2207-2226 (2015).
18 de Miró, M. D. Los foraminiferos planctónicos vivos y sedimentados del margen continental de Venezuela (resumen). *Acta geológica hispánica* **6**, 102-108 (1971).
19 Tedesco, K. A. & Thunell, R. C. Seasonal and interannual variations in planktonic foraminiferal flux and assemblage composition in the Cariaco Basin, Venezuela. *The Journal of Foraminiferal Research* **33**, 192-210 (2003).
20 Bova, S., Rosenthal, Y., Liu, Z., Godad, S. P. & Yan, M. Seasonal origin of the thermal maxima at the Holocene and the last interglacial. *nature* **589**, 548-553 (2021).
21 Rühlemann, C., Mulitza, S., Müller, P. J., Wefer, G. & Zahn, R. Warming of the tropical Atlantic Ocean and slowdown of thermohaline circulation during the last deglaciation. *Nature* **402**, 511-514, doi:Doi 10.1038/990069 (1999).
22 Haug, G. H., Hughen, K. A., Sigman, D. M., Peterson, L. C. & Rohl, U. Southward migration of the intertropical convergence zone through the Holocene. *Science* **293**, 1304-1308, doi:DOI 10.1126/science.1059725 (2001).
23 Rasmussen, S. O. *et al.* A stratigraphic framework for abrupt climatic changes during the Last Glacial period based on three synchronized Greenland ice-core records: refining and extending the INTIMATE event stratigraphy. *Quaternary Science Reviews* **106**, 14-28 (2014).
24 Rayner, N. *et al.* Global analyses of sea surface temperature, sea ice, and night marine air temperature since the late nineteenth century. *Journal of Geophysical Research: Atmospheres* **108** (2003).
25 Enfield, D. B., Mestas-Nuñez, A. M. & Trimble, P. J. The Atlantic multidecadal oscillation and its relation to rainfall and river flows in the continental US. *Geophysical Research Letters* **28**, 2077-2080 (2001).
26 Lee, S. K., Enfield, D. B. & Wang, C. Why do some El Ninos have no impact on tropical North Atlantic SST? *Geophysical Research Letters* **35**, doi:10.1029/2008gl034734 (2008).
27 Park, J.-H. & Li, T. Interdecadal modulation of El Niño–tropical North Atlantic teleconnection by the Atlantic multi-decadal oscillation. *Climate Dynamics* **52**, 5345-5360 (2019).
28 Laskar, J. *et al.* A long-term numerical solution for the insolation quantities of the Earth. *Astron Astrophys* **428**, 261-285 (2004).